CAPACITY OF MONO-SYMMETRIC GIRDERS WITH SLENDER WEBS IN PLATE GIRDER COMPOSITE BRIDGES

Ghada M. El-Mahdy*

ABSTRACT

Mono-symmetric plate girders are often used in simply supported composite bridges to eliminate local plate buckling in the compression flange during construction. This causes the neutral axis of the plate girder to shift downwards subjecting more of the web to compressive stresses due to bending. In slender webs this increases the possibility of local buckling in the compression part of the web during construction. However, depending on the slenderness (width-to-thickness ratio) of the web, the post-buckling reserve capacity may accommodate this local buckling within the elastic limit of the web for during construction loads. Hence, this would allow for the use of more slender webs in composite plate girder construction without the need for longitudinal web stiffeners or the reduction of the overall composite section due to local plate buckling in the web. Recommended values of stress level are given for mono-symmetric plate girders in the non-composite stage based on the results of a non-linear finite element analysis.

Keywords: composite bridges, effective width, finite element analysis, local plate buckling, mono-symmetric sections, plate girders, stress gradient, stress level.

1- INTRODUCTION

Plate girders in conjunction with a reinforced concrete slab are often used as composite plate girder bridges in positive bending. This has the advantage of reducing the possibility of local plate buckling in the plate girder's web and compression flange as a result of composite action under service loads. In addition to this, the during construction loads acting on the plate girder section alone, DL_1, may be designed to allow for local buckling in the web while keeping the stresses within the elastic limit of the plate girder section during construction.

For plate girders with webs having a width-to-thickness ratio in the *very* slender range, the critical stress is well below the yield stress, and under the effect of construction loads only, Fig. (1-a), the post-buckling state of the slender web may cause a nonlinear stress distribution, but the stresses in the web may still be in the elastic range. This would allow for the use of more slender webs for composite plate girders keeping in mind that the neutral axis will shift upwards with the onset of composite action, as shown in Fig. (1-b). Hence, preventing residual strains due to the yielding of the section during the construction non-composite stage and the after construction composite stage. The stress distribution for both the non-composite and composite stages for un-shored construction is shown in Fig. (1).

Other researchers to study composite I-girders are Gupta [1], Gupta *et al.* [2], Basker *et al.* [3], and Yakel and Azizinamini [4].

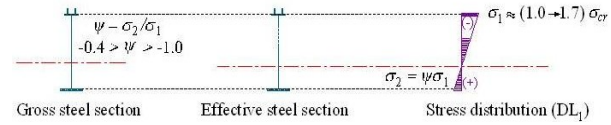

a- Un-shored non-composite section with ineffective concrete slab (DL_1 only)

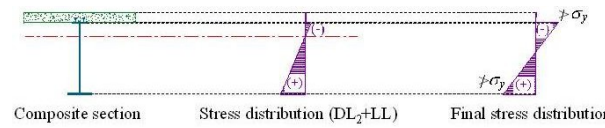

Un-shored composite section after gardening of concrete slab (DL_1 + DL_2+LL)

Fig. 1- Stress distribution in composite construction

* *Associate Research Professor, Structures and Metallic Construction Research Institute, Housing and Building National Research Center (HBRC), Egypt*

2- LOCAL PLATE BUCKLING

Local plate buckling occurs in slender plate elements when the compressive stress in the plate element exceeds the critical plate buckling stress of the plate element, as shown in Fig. (2), after the onset of plate buckling, a wave-like propagation of out-of-plane deformations breaks out increasing in amplitude with the increase in loading. This causes the compressive stresses to redistribute in the plate element, concentrating in the regions supported by stable boundary conditions. Due to the loss of in-plane stiffness of the unsupported regions, compressive and tensile bending stresses develop through the thickness of the plate, fluctuating along the length of the plate. The stress at the stable edges gradually increases with the increase in loading after the onset of local buckling up to the yield stress, σ_y. Once the edge stress has reached the yield stress, the plasticization of the plate element propagates in the nearby regions till the supported parts of the plate element are assumed to have reached the yield stress. Whereas, the unsupported unstable internal part of the plate element is assumed to be ineffective. Hence, the plate element does have a post-buckling reserve capacity which can be within the elastic limit of the element if the edge stress does not reach the yield stress capacity.

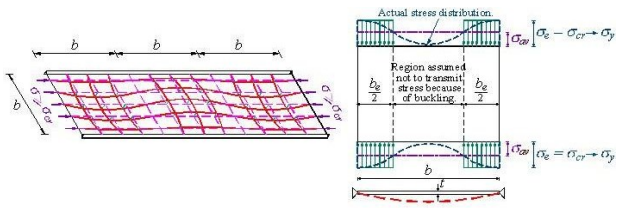

Fig.2 - Concept of effective width

The elastic buckling stress, σ_{cr}, of slender plates as derived by von Kàrmàn *et al.* [5] is:

$$\sigma_{cr}=\frac{k\pi^2 E}{12(1-\nu^2)}\left(\frac{t}{b}\right)^2 \quad \text{..... (1)}$$

which is inversely proportional to the square of the width-to-thickness ratio, b/t, of the plate element. The plate buckling factor, k, depends on the longitudinal boundary conditions of the plate element and the normal stress distribution in the plate, $\Psi = \sigma_2/\sigma_1$, shown in Fig. (1). Expressions for k for different boundary conditions can be found in the Eurocode EC3 EN 1993-1-1:2003 [6] or the Egyptian Code of Practice for Steel Construction and Bridges ECOP-ASD [7]. The modulus of elasticity, E, can be taken as 210,000 MPa and Poisson's ratio, ν, can be taken as 0.3.

From the expression for the uniform elastic critical stress, given in Eq. (1), acting on a plate with a width-to-thickness ratio of b/t we get:

$$\left(\frac{b}{t}\right)=\sqrt{\frac{k\pi^2 E}{12(1-\nu^2)\sigma_{cr}}} \quad \text{..... (2)}$$

Assuming an effective width of b_e and a uniform stress acting on it of σ_e, which can have a value anywhere from the critical stress σ_{cr} to the yield stress σ_y as shown in Fig. (2), then by analogy we get:

$$\left(\frac{b_e}{t}\right)=\sqrt{\frac{k\pi^2 E}{12(1-\nu^2)\sigma_e}} \quad \text{..... (3)}$$

Hence, the ratio of the effective width b_e, to the original width b, known as the effective width parameter ρ, is:

$$\rho=\left(\frac{b_e}{b}\right)=\sqrt{\frac{\sigma_{cr}}{\sigma_e}} \quad \text{..... (4)}$$

Assuming that the average uniform stress of the nonlinear post-buckling stress distribution is σ_{av} as shown in Fig. (2), the effective width is assumed to be the width subject to a stress equal to the edge stress, σ_e, of the nonlinear stress distribution such that it develops a strength equal to the average stress acting on the whole width.

Hence,

$$b_e\sigma_e=b\sigma_{av} \quad \text{..... (5)}$$

giving:

$$\sigma_{av}=\left(\frac{b_e}{b}\right)\sigma_e=\sqrt{\sigma_{cr}\sigma_e} \quad \text{..... (6)}$$

Taking the non-dimensional slenderness parameter λ_n as:

$$\lambda_n=\sqrt{\frac{\sigma_e}{\sigma_{cr}}}=\sqrt{\frac{12(1-\nu^2)}{k\pi^2}}\frac{b}{t}\sqrt{\frac{\sigma_e}{E}} \quad \text{.....(7)}$$

and substituting this into Eq. (6) gives:

$$\sigma_{av}=\frac{1}{\lambda_n}\sigma_e \quad \text{..... (8)}$$

To account for the effect of residual stresses in the moderately slender and the non-compact

slenderness ranges, the American Iron and Steel Institute (AISI) [8] suggests the following expression for the average stress.

$$\sigma_{av}=\frac{\lambda_n-0.22}{\lambda_n^2}\sigma_e \quad \text{..... (9)}$$

Both Eqs. (8, 9) are plotted in Fig. (3).

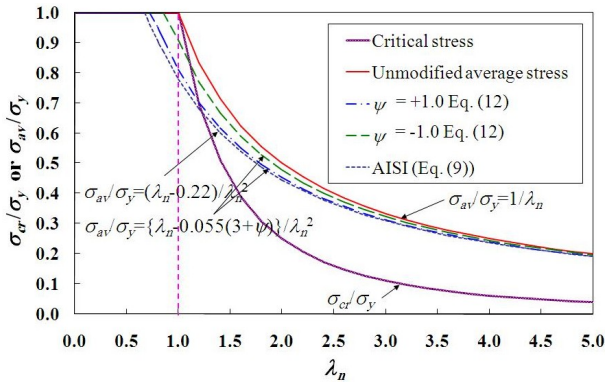

Fig. 3- Normalized plate buckling curves

3 - EFFECT OF STRESS GRADIENT ON LOCAL PLATE BUCKLING

To include the effect of stress gradient in the plate element due to combined compressive and flexural stresses in the member, as shown in Fig. 4, the effective width parameter, ρ, is assumed to take the form:

$$\frac{\sigma_{av}}{\sigma_e}=\frac{b_e}{b}=\rho=\frac{\lambda_n-x-y\psi}{\lambda_n^2} \quad \text{..... (10)}$$

Where x and y can be determined from the limits of b/t for *stiffened* slender plate elements in pure compression, Ψ = +1.0, and pure bending, Ψ = -1.0.

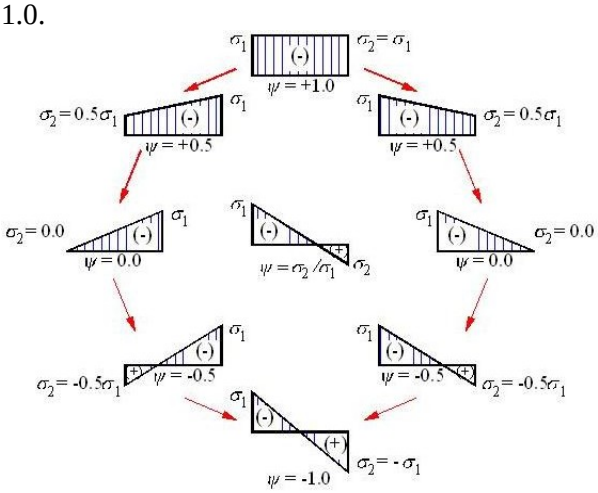

Fig. 4- Schematic representation of stress gradient, Ψ, due to combined compressive and flexural stresses

This is the same method used by El-Mahdy and Abu-Hamd [9, 10, and 11] to derive the current equation for the effective width of stiffened slender plate elements subject to a stress gradient in the Egyptian Code of Practice for the Design of Steel Construction and Bridges [7]. For example, using the limits for pure compression and pure bending given in the Eurocode EC3 [6],

$$\frac{b}{t}=42\varepsilon \quad for \quad \psi=+1.0$$
$$\frac{b}{t}=124\varepsilon \quad for \quad \psi=-1.0 \quad \text{..... (11)}$$

Where:

$$\varepsilon=\sqrt{235/\sigma_y}$$

and taking

k = 4.0 for the case of pure compression and k = 23.9 for the case of pure bending and assuming $\sigma_e = \sigma_y$ gives the values 0.144 and 0.048 for x and y, respectively. Hence, according to the limits of the EC3 [6]:

$$\frac{\sigma_{av}}{\sigma_e}=\frac{b_e}{b}=\rho=\frac{\lambda_n-0.144-0.048\psi}{\lambda_n^2} \quad \text{..... (12)}$$

Factorizing and approximating this leads to the expression:

$$\frac{\sigma_{av}}{\sigma_e}=\frac{b_e}{b}=\rho=\frac{\lambda_n-0.05(3+\psi)}{\lambda_n^2} \quad \text{..... (13)}$$

which is close to the expression given in the EC3 EN 1993-1-5:2006 [12].

$$\frac{\sigma_{av}}{\sigma_e}=\frac{b_e}{b}=\rho=\frac{\lambda_n-0.055(3+\psi)}{\lambda_n^2} \quad \text{..... (14)}$$

The normalized average stress for the cases of Ψ = +1.0 and Ψ = -1.0, according to Eq. (12), are plotted in Fig. (3).

4 - FINITE ELEMENT ANALYSIS

A finite element parametric analysis, using COSMOS 2.6 software, is conducted on models of plate girders having a web depth of 1000 mm and varying the web thickness, t_w, from 5 mm to 11 mm giving a width-to-thickness ratio for the web varying from 200 to 91. The compression flange is kept constant in the non-compact range having a size of 200 x 11 mm, whereas, the size of the tension flange is increased to achieve a stress gradient in the web of Ψ = -1.0, -0.8, -0.6, and -0.4, as shown in Fig. (5).

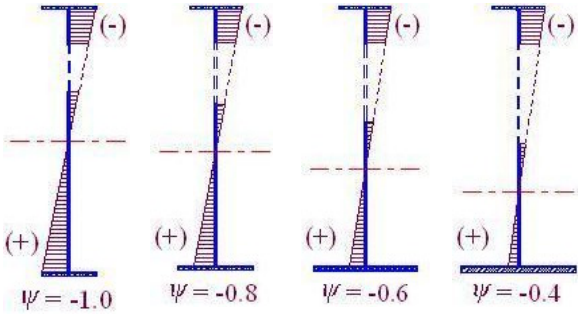

Fig. 5- Schematic representation of parametric plate girder cross-sections

A model with a simply supported span of length L = 10 m is used. In the actual finite element model the height of the web is modelled having a depth of 1000 mm plus half the thickness of both the compression flange and the tension flange. This causes a slight decrease of the stress gradient in the web due to a minor change in the position of the model's neutral axis, but this decrease is negligible. Both flanges are laterally supported as shown in Fig. (6 -a) to prevent any out-of-plane lateral torsional-flexural buckling occurring in the compression flange. Elastic-plastic shell elements are used to model the flange and web plate elements, however, the end parts of the top and bottom flanges are stiffened by increasing their thickness and taken as elastic shell elements to overcome local deformations due to loads applied to these flanges. The material of the model is taken as elastic-perfectly plastic with a modulus of elasticity of 210 GPa and a yield stress of 350 MPa.

The compression and tension flanges of each model are loaded to cause a moment equal to the yield capacity of the section. This is achieved by applying equivalent end compression and tension forces in the top and bottom flanges, respectively, according to the following formulas:

$$F_{et} = A_{tf} F_y \left(1 + \frac{A_w}{A_{tf}} \frac{1}{3(1-\psi)} \right) \quad \text{.....} \quad (15)$$

$$F_{eb} = A_{bf} (-\psi) F_y \left(1 + \frac{A_w}{A_{bf}} \frac{-\psi}{3(1-\psi)} \right) \quad \text{.....} \quad (16)$$

This gives a yield moment, M_y, of:

$$M_y = h_w F_y \left(\frac{A_{tf} + \psi^2 A_{bf}}{(1-\psi)} + \frac{A_w}{3} \frac{1+(-\psi)^3}{(1-\psi)^2} \right) \quad ..(17)$$

Where:

F_{et} and F_{eb} are the equivalent compression and tension forces assumed to be concentrated at the centroids of the flanges that cause a moment equal to the yield moment capacity of the section, respectively; A_{tf} and A_{bf} are the areas of the top and bottom flange plates, respectively; and h_w and A_w are the depth and area of the model's web plate, respectively.

The results of the linear analysis conducted on the finite element models verify that the gross stiffness of the model, calculated from the midpoint deflection, Δ, compare accurately with the analytic expression for a simply supported beam subject to a uniform moment, M, *viz.*, $I = ML^2/8E\Delta$. The position of the neutral axis can also be determined from the normal stress distribution in the deflected model. Excessive stresses are noted in the flanges near the loaded edges. Figure (6-b) shows the normal stress distribution in the deformed model with a web thickness of 5 mm or a web slenderness of 200 and a bottom flange sized to give a stress gradient of Ψ = -0.6.

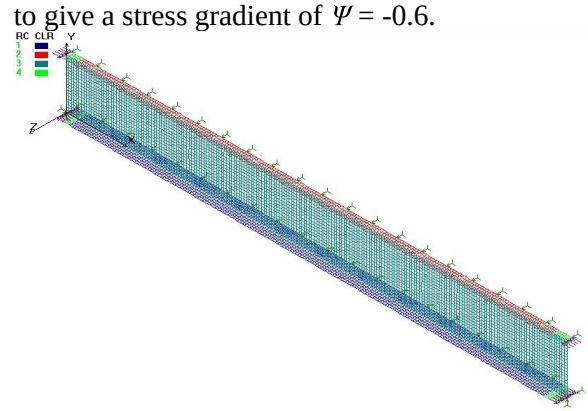

a- Finite element model

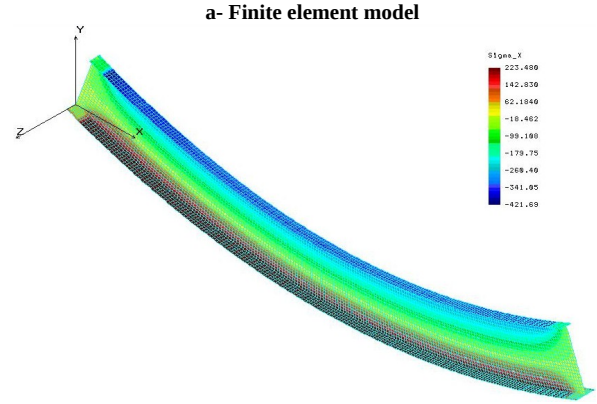

b- Deformed shape and stress distribution

Fig. 6- Typical finite element model and normal stress distribution of linear analysis

A nonlinear analysis which follows the

Newton-Raphson incremental-iterative procedure is used to detect the propagation of local plate buckling in the slender web. An initial 1 mm out-of-flatness at the center-point of the web is used in the model to initiate local web buckling.

Finally, a finite element analysis of the composite section, shown in Fig. (7), using a slab of 2000 x 200 mm with a concrete cube strength, f_c', of 40 MPa and uniformly loaded above the slab gave approximate values of the residual capacity of the composite section in the after construction phase.

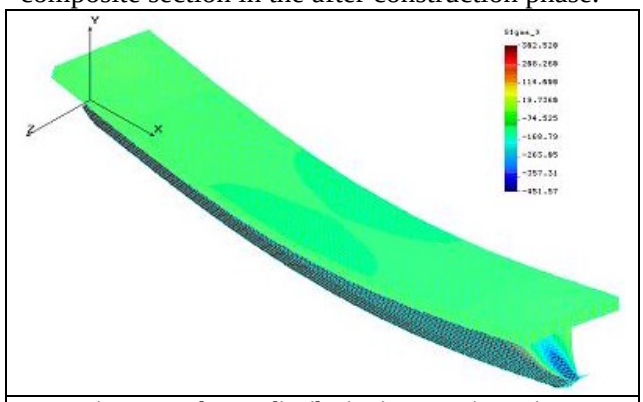

Fig7- Normal stress distribution in composite section

5- DISCUSSION OF RESULTS

Figure (8) illustrates the in-plane membrane normal stress distribution and the out-of-plane local plate buckling of the web in flexural compression for the model with a web slenderness of 200 (*i.e.*, t_w = 5 mm) and a stress ratio of Ψ = -0.6. At a stress level of $1.72\sigma_{cr}$, shown in Fig. (8-a), it can be seen that a notable amount of local buckling in the compression part of the web has occurred without causing any distortional buckling in the non-compact adjacent compression flange, and without exceeding the elastic limit as shown by the maximum compressive stress of 146 MPa. Whereas, for a stress level of σ_y= 350 MPa, shown in Fig. (8-b), the local buckling of the web in compression is greatly magnified causing distortional buckling in the adjacent compression flange. Figure (8-c) shows the stress distribution along the web for the same model at different stress levels. It can be seen that the stress distribution along the web remains relatively linear even after local buckling has initiated at the critical stress level, however, considerable nonlinearity in the stress distribution occurs near the end of the nonlinear analysis as the stress level approaches the yield stress. This is also demonstrated by the load-deflection curves shown in Fig. (8-d). It can also be noted that the neutral axis tends to shift upwards with the occurrence of local plate buckling in the web and the nonlinear stress distribution.

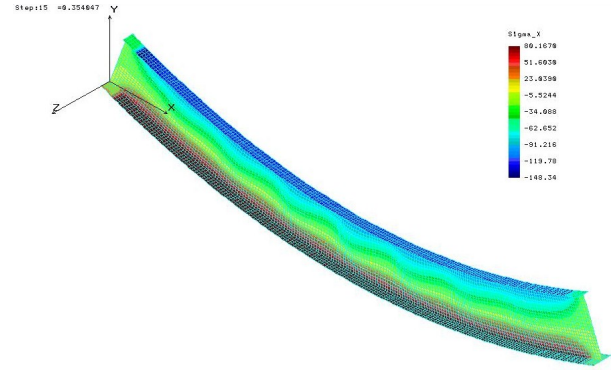

a- Stress level $1.72\sigma_{cr}$

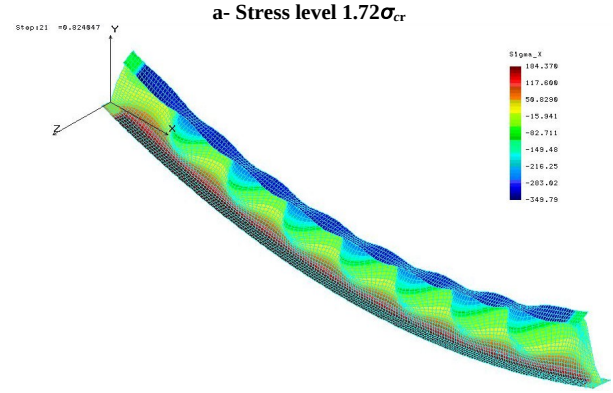

b- Stress level σ_y

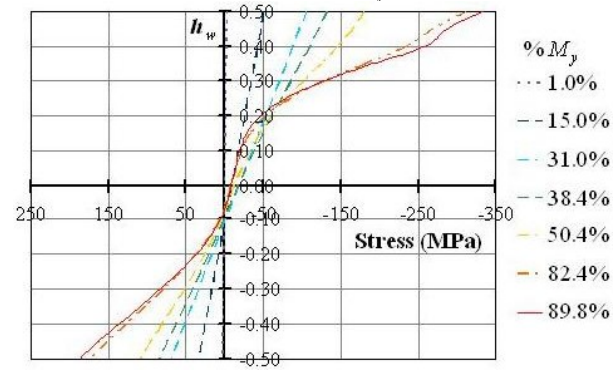

c- Stress distribution along the web at different stress levels

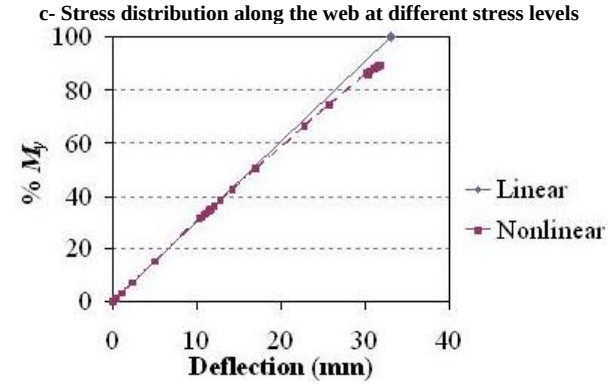

d- Load-deflection curves

Fig. 8- Deformed shape and normal membrane stress distribution for model with web slenderness 200 and Ψ = -0.6

Figure (9) shows the deformed shape and normal membrane stress distribution for the model with a web slenderness of 125 (*i.e*, t_w = 8 m) and a bottom flange proportioned to give a stress ratio of Ψ = -0.6. A slight amount of local web buckling can be detected at a stress level of $1.47\sigma_{cr}$ where the maximum compressive stress is 337 MPa and hence is still below the yield stress, as shown in Fig. (9-a). However, at a stress level of σ_y the local buckling in the web is magnified causing distortional buckling in the compression flange, as shown in Fig. (9-b.c) shows the stress distribution along the web for this model at different stress levels. It can be seen that the stress distribution along the web remains relatively linear even after local buckling has initiated at the critical stress level, however, a slight nonlinearity in the stress distribution occurs near the end of the nonlinear analysis as the stress level approaches the yield stress. The slight nonlinearity is again shown in the load-deflection curve in Fig. (9-d).

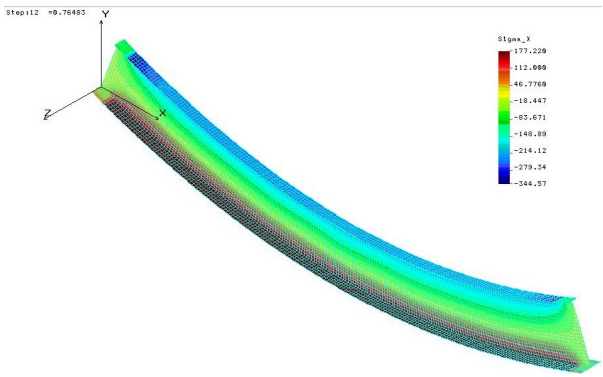

a- Stress level $1.47\sigma_{cr}$

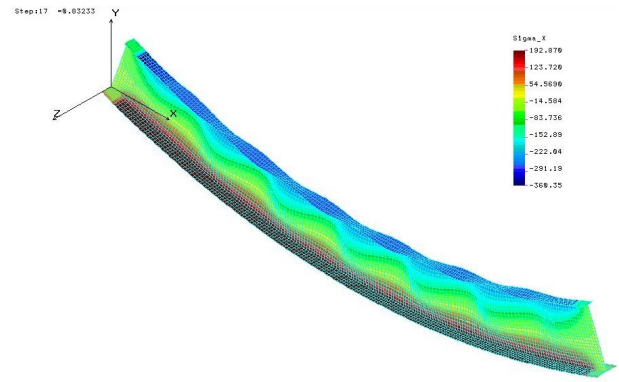

b- Stress level σ_y

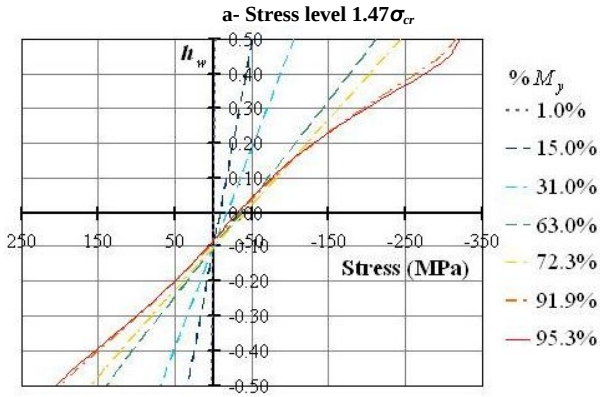

c- Stress distribution along the web at different stress levels

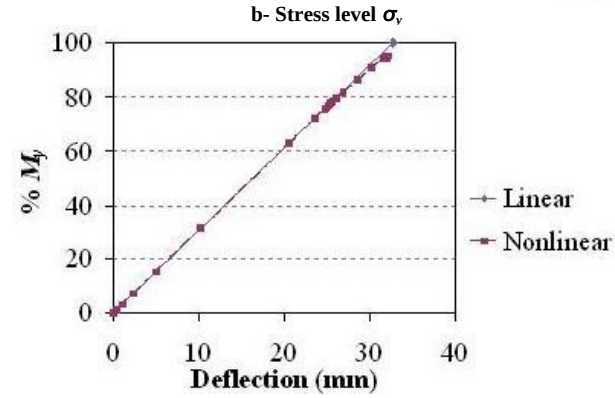

d- Load-deflection curves

Fig. 9- Deformed shape and normal membrane stress distribution for model with web slenderness 125 and Ψ = -0.6

Finally, Fig. (10), shows the deformed shape and normal stress distribution for the model with a web slenderness of 100 (*i.e.*, t_w = 10 mm) and a lower flange proportioned to give a stress ratio of Ψ = -0.6. At a stress level of $\approx \sigma_{cr}$ the maximum stress is close to σ_y and very little local web buckling has occurred, as shown in Fig. (10a). In fact, at a stress level of $1.09\sigma_y$ the local buckling is still hard to detect although the section has yielded, as shown in Fig. (10-b, c) shows the stress distribution along the web for this model at different stress levels. It can be seen that the stress distribution along the web remains linear up to the end of the nonlinear analysis as the stress level approaches the yield stress. This linearity is also depicted in the load-deflection curves shown in Fig. (10 d).

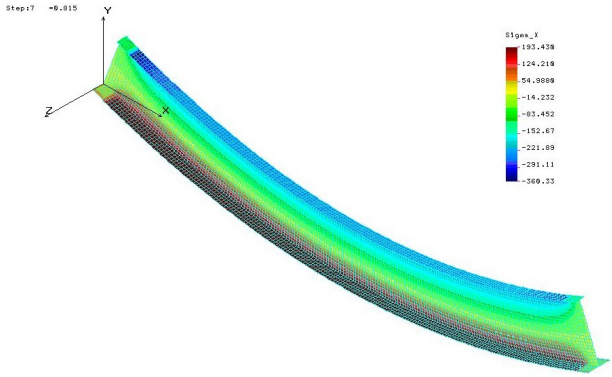

a- Stress level $\approx\sigma_{cr}$

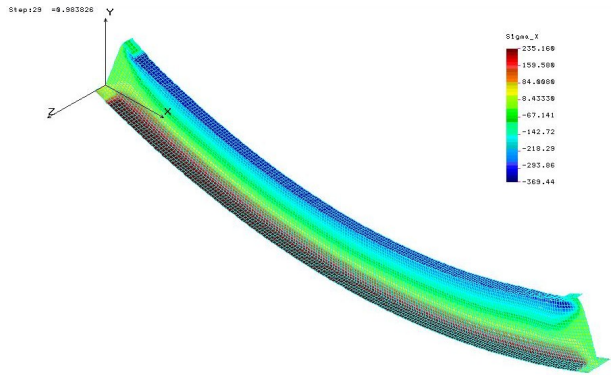

b- Stress level $1.09\sigma_y$

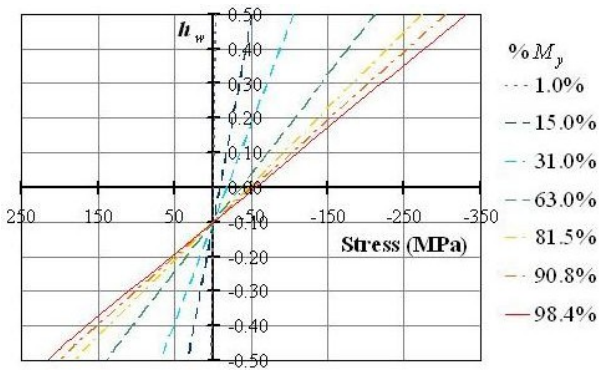

c- Stress distribution along the web at different stress levels

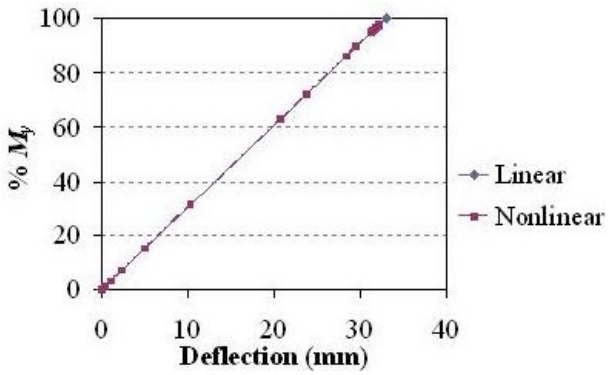

d- Load-deflection curves

Fig. 10- Deformed shape and normal membrane stress distribution for model with web slenderness 100 and Ψ = -0.6

The recommended values of stress level with respect to the critical stress for other stress gradients as determined by the nonlinear finite element analysis are listed in Table 1 and are plotted in Fig. (11).

Table 1- Recommended values of stress level

Ψ \ h_w/t_w	200	167	143	125	111	100
-1.0	1.56	1.5	1.39	1.00	-	-
-0.8	1.64	1.59	1.49	1.36	1.00	-
-0.6	1.72	1.63	1.57	1.47	1.35	1.00
-0.4	1.76	1.68	1.6	1.54	1.44	1.16

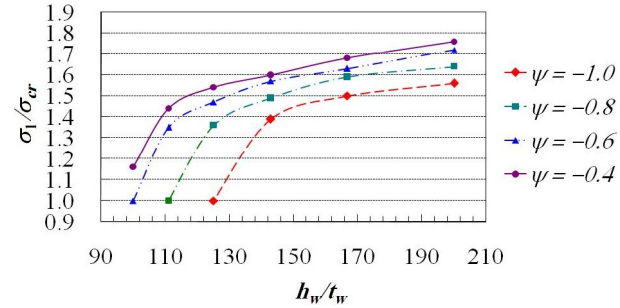

Fig. 11- Recommended values of stress level for mono-symmetric girders

From the finite element results of the composite sections, it can be noted that increasing the thickness of the web results in a minor increase in composite capacity. Whereas using a greater value of stress gradient (*i.e.*, Ψ = -0.4) greatly increases the composite capacity 2 – 3 times, and any loss in the capacity of the non-composite section due to the buckling of the slender web can be compensated for by using shoring during construction.

6- CONCLUSION

The finite element parametric analysis shows that mono-symmetric non-composite plate girders with slender webs can be stressed beyond the critical stress, initiating the onset of local buckling of the web in flexural compression, without exceeding the elastic limit. However, due to the occurrence of excessive local buckling deformations in slender webs causing distortional buckling in the compression flange, the following stress limits are recommended depending on the stress ratio in the web; $1.7\sigma_{cr}$ for webs in the *very* slender range decreasing to $1.0\sigma_{cr}$ for webs in the *less* slender range.

REFERENCES

[1] Gupta, V.K., "Development of section classification criterion and ultimate flexural equation for composite I-girders", Doctoral Dissertation, Saitama University, Japan, 2006.

[2] Gupta, V.K., Yoshiaki, O., and Nagai, M., "Development of web slenderness limits for composite I-girders accounting for initial bending moment", Doboku Gakkai Ronbunshuu A (JSCE Journal of Structural and Earthquake Engineering), Vol. 62, No. 4, pp. 854-864, 2006.

[3] Basker, K., Shanmugan, N.E., and Thevendran, V., "Finite-element analysis of steel-concrete composite plate girder", J. Struct. Eng., ASCE, Vol. 128, No. 9, pp. 1158-1168, 2002.

[4] Yakel, A.J. and Azizinamini, A., "Improved moment strength prediction of composite steel plate girders in positive bending", J. Bridge Eng., ASCE, Vol. 10, No. 1, pp. 28-38, 2005.

[5] Von K?rm?n, T., Sechler, E.E., and Donell, L.H., "Strength of thin plates in compression", Transactions of the American Society of Mechanical Engineers, Vol. 54, No. APM-54-5, p. 53, 1932.

[6] Eurocode 3, Design of steel structures – Part 1.1 General structural rules (EN 1993-1-1:2003), European Committee for Standardization (CEN), Brussels, Belgium, 2005.

[7] ECOP-ASD, Egyptian Code of Practice for Steel Construction and Bridges – Allowable Stress Design, Egypt, 2001.

[8] American Iron and Steel Institute, Specification for the design of cold-formed steel structural members, AISI, Washington DC, 2007.

*[9] Abu-Hamd, M.H. and Elmahdy, G.M., "The effective width of slender plate elements in plate girders", Journal of Engineering and Applied Science, Faculty of Engineering - Cairo University, **50**(2): 259-278, 2003.*

[10] Elmahdy, G. and Abu-Hamd, M., "New formula for the effective width of slender plate elements", Proceedings of the CSCE Annual Conference - 6th Structural Speciality Conference, Quebec City, Quebec, Canada, 2008.

[11] El-Mahdy, G. and Abu-Hamd, M., "Local buckling of slender plate girders in composite bridges", Proceedings of the SSRC Annual Stability Conference, Orlando, Florida, USA, 2010.

[12] Eurocode 3, Design of steel structures – Part 1.5 Plated structural elements (EN 1993-1-5:2006), European Committee for Standardization (CEN), Brussels, Belgium, 2006.